Cell Reports

Resource

Human amyotrophic lateral sclerosis excitability phenotype screen: Target discovery and validation

Graphical abstract

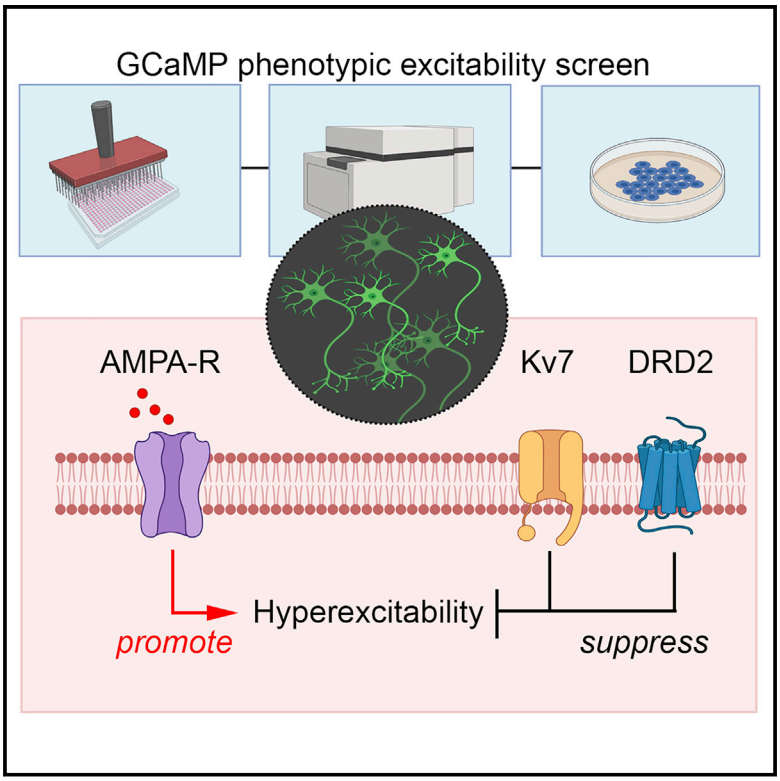

Authors

Xuan Huang, Kasper C.D. Roet, Liying Zhang, ..., Seungkyu Lee, Kevin Eggan, Clifford J. Woolf

Correspondence

clifford.woolf@childrens.harvard.edu

In brief

Motor neuron hyperexcitability is observed in both ALS patients and their iPSC-derived neurons. Combining a high-content live imaging excitability phenotypic assay, high-throughput screening against a cross-annotated chemogenomic library, and bioinformatic enrichment analysis, Huang et al. identify targets modulating the hyperexcitability of ALS patient-derived motor neurons in an unbiased manner.

Highlights

- ALS patient-derived motor neurons are hyperexcitable
- A high-throughput GCaMP screen is used to identify ALS excitability modulators
- Kv7 ion channels, AMPA receptors, and the type 2 dopamine receptor are major targets
- The D2 dopamine receptor modulates both neuronal excitability and survival

Huang et al., 2021, Cell Reports *35*, 109224
June 8, 2021
https://doi.org/10.1016/j.celrep.2021.109224

CellPress

Cell Reports

CellPress
OPEN ACCESS

Resource

Human amyotrophic lateral sclerosis excitability phenotype screen: Target discovery and validation

Xuan Huang,[1,8] Kasper C.D. Roet,[1,8] Liying Zhang,[2] Amy Brault,[3] Allison P. Berg,[4] Anne B. Jefferson,[5,9] Jackie Klug-McLeod,[2] Karen L. Leach,[6,10] Fabien Vincent,[3] Hongying Yang,[6] Anthony J. Coyle,[6,11] Lyn H. Jones,[2,12] Devlin Frost,[1] Ole Wiskow,[7] Kuchuan Chen,[1] Rie Maeda,[1] Alyssa Grantham,[1] Mary K. Dornon,[1] Joseph R. Klim,[7] Marco T. Siekmann,[1,13] Dongyi Zhao,[1] Seungkyu Lee,[1] Kevin Eggan,[7] and Clifford J. Woolf[1,14,*]

[1]F.M. Kirby Neurobiology Center, Boston Children's Hospital, and Department of Neurology, Harvard Medical School, 300 Longwood Avenue, Boston, MA 02115, USA
[2]Medicine Design, Pfizer, Cambridge, MA 02139, USA
[3]Medicine Design, Pfizer, Groton, CT 06340, USA
[4]Rare Disease Research Unit, Pfizer, Cambridge, MA 02139, USA
[5]Pfizer Centers for Therapeutic Innovation (CTI), San Francisco, CA 94080, USA
[6]Pfizer Centers for Therapeutic Innovation (CTI), Cambridge, MA 02139, USA
[7]Department of Stem Cell and Regenerative Biology, Department of Molecular and Cellular Biology, Harvard Stem Cell Institute, Cambridge, MA 02138, USA
[8]These authors contributed equally
[9]Present address: Biopharmaceutical Consultant, Farmville, VA, USA
[10]Present address: MolPharm Consulting, West Haven, CT, USA
[11]Present address: Repertoire immune medicine, Cambridge, MA, USA
[12]Present address: Dana-Farber Cancer Institute, Boston, MA 02215, USA
[13]Present address: Hector Institute for Translational Brain Research (HITBR gGmbH), Central Institute of Mental Health, University of Heidelberg, Heidelberg, Germany
[14]Lead contact
*Correspondence: clifford.woolf@childrens.harvard.edu
https://doi.org/10.1016/j.celrep.2021.109224

SUMMARY

Drug development is hampered by poor target selection. Phenotypic screens using neurons differentiated from patient stem cells offer the possibility to validate known and discover novel disease targets in an unbiased fashion. To identify targets for managing hyperexcitability, a pathological feature of amyotrophic lateral sclerosis (ALS), we design a multi-step screening funnel using patient-derived motor neurons. High-content live cell imaging is used to evaluate neuronal excitability, and from a screen against a chemogenomic library of 2,899 target-annotated compounds, 67 reduce the hyperexcitability of ALS motor neurons carrying the *SOD1(A4V)* mutation, without cytotoxicity. Bioinformatic deconvolution identifies 13 targets that modulate motor neuron excitability, including two known ALS excitability modulators, AMPA receptors and Kv7.2/3 ion channels, constituting target validation. We also identify D2 dopamine receptors as modulators of ALS motor neuron excitability. This screen demonstrates the power of human disease cell-based phenotypic screens for identifying clinically relevant targets for neurological disorders.

INTRODUCTION

Phenotypic screening assays use the modulation of a cellular phenotype (e.g., survival, morphology, or gene expression) rather than a change in function of a specific protein as its output (Vincent et al., 2015). This strategy can identify compounds that interfere with disease pathogenesis that, in turn, from the compound's known biological activity, can elucidate new targets/pathways related to disease pathology or those that can modify disease. Target discovery for diseases with multiple, complex, and dynamic phenotypes can therefore be greatly aided by optimally designed phenotypic screens using relevant human patient-derived cells. Chemogenomic libraries comprising small molecules with known specific biological activity (Jones and Bunnage, 2017; Cong et al., 2012) can be utilized to study the normalization of disease phenotypes and in this way reveal individual targets that participate in disease-promoting pathways. Compared with genomic interference strategies such as RNAi and CRISPR knockout/knockdown, a chemogenomic library may minimize compensatory changes and overcome gene redundancy and is technically easier to use, especially for human neuron phenotypic assays. Use of such libraries provides an unbiased approach to teasing out drug targets that drive disease phenotypes.

Amyotrophic lateral sclerosis (ALS) is a lethal neurodegenerative disorder that is characterized by loss of adult motor neurons and that currently lacks effective treatment. Multiple potential mechanisms have been proposed (Robberecht and Philips, 2013; Kanning et al., 2010), and many of these pathological disturbances are recapitulated in human motor neurons differentiated from patient induced pluripotent stem cell (iPSC) lines, which in consequence are emerging as a powerful human cell-based system for disease modeling and drug discovery (Bilican et al., 2012; Donnelly et al., 2013; Kiskinis et al., 2014; Wainger et al., 2014; Lopez-Gonzalez et al., 2016). As patient iPSC-derived motor neurons reflect key features of ALS and can be generated in large amounts, several attempts have been made to identify pathways that protect against cell death (Imamura et al., 2017; Yang et al., 2013). Novel phenotypic screens could expand ALS drug development to target new features that increase susceptibility to neurodegeneration.

We have now conducted a neuronal phenotypic screen using iPSC-derived motor neurons from patients with ALS for a reduction in intrinsic hyperexcitability, a prominent clinical phenotype that has not been studied in a high-throughput manner. Neuronal hyperexcitability is observed in multiple different ALS models and contributes to cell toxicity by calcium overload (King et al., 2016). In patients, increased motor axonal excitability is revealed by *in vivo* excitability assessments such as threshold tracking (Park et al., 2017; Wainger et al., 2021), which reflects aberrant sodium and potassium currents. An increase in excitability in patients is associated with muscle cramps and fasciculations and most importantly, shorter survival (Nakata et al., 2006; Kanai et al., 2012). Previously, we found that patient-derived motor neurons harboring *SOD1*, *FUS*, or *C9ORF72* mutations are hyperexcitable relative to healthy motor neurons and that this is associated with an increased vulnerability to cell death (Kiskinis et al., 2014; Wainger et al., 2014). This *in vitro* recapitulation of the clinical phenotype suggests that differentiated human motor neurons can be utilized to identify therapies to modulate pathological hyperexcitability in patients with ALS (Wainger et al., 2021). However, to achieve this, certain technical problems need to be overcome to make the assay robust, sensitive, reliable, and suitable for a high-throughput format.

Our goal here was to develop a high-content screen against annotated compounds to identify major molecular targets that modify hyperexcitability in human motor neurons carrying the *SOD1(A4V)* familial ALS mutation (Kanai et al., 2012; Shibuya et al., 2016; Iwai et al., 2016). As traditional electrophysiology techniques such as patch-clamp or multielectrode array (MEA) recordings are not suitable for unbiased high-throughput screening in large plate format, we developed a live single-cell calcium reporter (GCaMP, a genetically encoded calcium indicator) screening platform. Through multiple rounds of screening, we identified 67 compounds that effectively decrease neuronal excitability without cytotoxicity, from a well-annotated, 2,899-compound chemogenomic library (Jones and Bunnage, 2017). Target deconvolution utilizing the multiple cross-annotations of the compounds confirmed AMPA receptors and Kv7 potassium channels as two prime ALS hyperexcitability-reducing targets and revealed the D2 dopamine receptor as an ALS excitability modulator. This confirms the value of phenotypic screens for identification of targets that modulate a disease phenotype.

RESULTS

High-content GCaMP imaging to measure motor neuron excitability

To model the ALS hyperexcitability disease phenotype *in vitro*, we used human motor neurons differentiated from a patient iPSC line carrying the *SOD1(A4V)* mutation (Figures S1A and S1B) (Kiskinis et al., 2014). To study neuronal excitability, we co-cultured the differentiated motor neurons with mouse glia that promote neuronal maturation and action potential firing (Wainger et al., 2014). Three to four weeks after differentiation, cocultured motor neurons exhibit large sodium and potassium currents and display spontaneous action potential firing (Figures S1C and S1D), indicating these neurons are electrophysiologically mature. During action potential firing, voltage-dependent calcium channels are activated, leading to an activity-dependent calcium influx (Chen et al., 2012, 2013). We therefore explored whether intracellular calcium waves can be used for image-based, high-content/high-throughput screening of ALS motor neuron hyperexcitability.

To monitor calcium signals by live cell imaging, motor neurons were infected with a lentivirus encoding a hsyn-GCaMP6s construct (Figure 1A), and the frequency of calcium waves in neuronal soma was quantified by fluorescent change measurements (Figure 1B; Video S1). As the GCaMP6s reporter is controlled by a human synapsin promoter, only neuronal calcium signals were captured, and we were able to measure the activities of more than one hundred neurons per well. Calcium wave counts were extracted from raw fluorescent intensity signals (details in STAR Methods) and significantly decreased by the sodium channel blocker tetrodotoxin (TTX) (Figure 1C), indicating they were driven by action potential firing. We compared the calcium waves per cell and per well and found that *SOD1(A4V)* ALS motor neurons had more frequent waves (Figures 1D, 1E, and S1E) than their isogenic controls where the mutation is corrected ("Cor") (Kiskinis et al., 2014), while basal fluorescent intensity stayed the same, showing that the GCaMP signal captures the pathological hyperexcitability observed by MEA recordings of action potential firing (Figure S1F). To further evaluate whether GCaMP signals can be used to assess compounds' effects on neuronal excitability, we tested 11 different commercially available ion channel modulators by both MEA and GCaMP recordings. The 8 MEA electrodes in each well recorded extracellular field potentials with a frequency of 20,000 Hz, while the calcium wave count was averaged from individual neurons in each well at 1 Hz. We found that the two approaches, extracellular action potential firing or intracellular calcium waves, showed similar activity reductions in response to the test compounds ($R^2 = 0.84$; $p < 0.0001$) (Table 1; Figure S1G). GCaMP signals in motor neurons can therefore be used to evaluate changes in intrinsic firing of motor neurons for *in vitro* hyperexcitability phenotypic screens.

Primary GCaMP screen

To find molecular targets modulating hyperexcitability with high fidelity, we set up a screening funnel including a primary and confirmation screen, followed by an efficacy/toxicity comparison, using a chemogenomic library generated by Pfizer where the

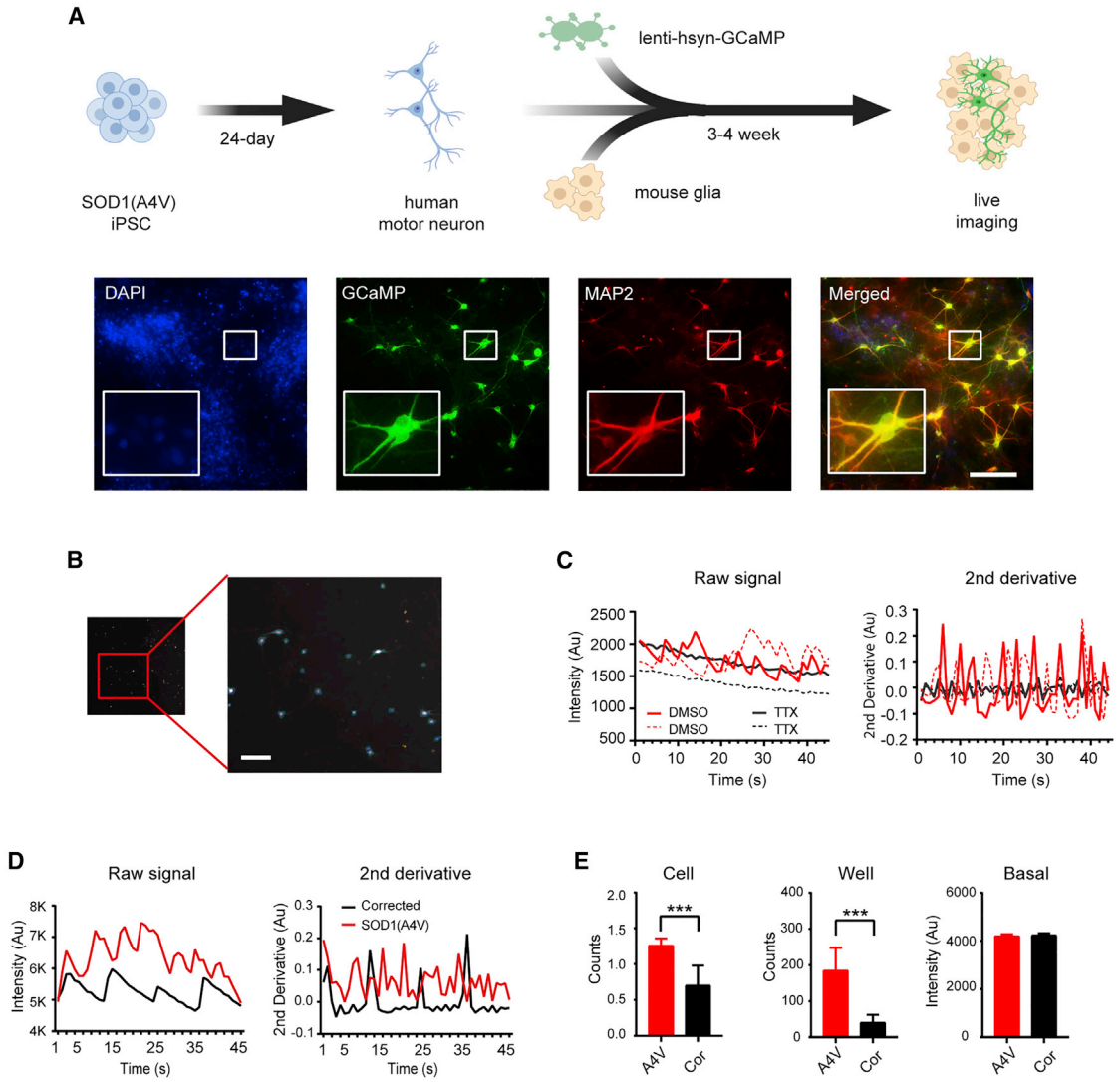

Figure 1. *In vitro* GCaMP assay to quantify human motor neuron excitability

(A) Embryonic body (EB)-differentiated *SOD1(A4V)* patient motor neurons were cocultured with mouse glia and infected by a lentivirus expressing GCaMP6s driven by the synapsin promoter. Three weeks after culture, cells were stained with DAPI, GCaMP, and Microtubule Associated Protein 2 (MAP2).

(B) Live imaging: somas of individual GCaMP-positive neurons were automatically detected, and somatic fluorescence intensity was measured at 1 Hz for 45 s.

(C) Examples of neuronal GCaMP activity. Raw signals from two TTX (5 μM)- and two DMSO-treated neurons as well as calculated 2nd derivative are demonstrated.

(D and E) GCaMP activity recorded from *SOD1(A4V)* and control motor neurons showing higher spontaneous activity in the diseased motor neurons. (D) Raw fluorescence intensity and corresponding 2nd derivative of one sample neuron from each genotype. (E) Quantified average calcium wave count per cell, total count per well, and basal fluorescence intensity at Day 18 in culture (D18) (n = 4–6 wells, ~360 different neurons from each genotype, mean ± SD, two-tailed t test). Scale bar, 100 μm. ***p ≤ 0.001. See also Figure S1 and Video S1.

compounds' mechanism of actions are fully characterized. The CGL3 library contains 2,899 compounds annotated for defined targets, including G-protein-coupled receptors (GPCRs), ion channels, multiple enzyme classes, and other families such as integrins and heat shock proteins (Figure S2A) (Jones and Bunnage, 2017). Notably, compounds in the library typically act on multiple targets, and in consequence, many targets covered by the library are acted on by more than five ligands. This target overlap/cross-annotation assists in target detection by enabling a bioinformatic enrichment analysis from the actions of multiple ligands (Figure S2B). ALS motor neurons carrying the *SOD1(A4V)* mutation (Kiskinis et al., 2014) were cocultured with glia in a 384-well plate format and infected with a GCaMP6s-encoding lentivirus. Between the 3rd and 4th week of coculture, a time when the motor neurons exhibit high levels of spontaneous activity (Figure S1D), compounds were added and GCaMP activity was recorded for 45 s at 1 Hz both at 6 and 24 h to capture targets that affect motor neuron excitability directly (e.g., via ion channels, at 6 h), and potentially through secondary effects (e.g., through altered transcription, at 24 h) (Figure 2A).

Table 1. Comparison of 11 ion channel modulators' effects on spontaneous motor neuron activity with GCaMP imaging and MEA

Compound	MEA (%)	GCaMP6 (%)	Target	Action
DMSO	100.00	100.00		
Maxipost (BMS-204352)	22.32 ± 1.1	36.67 ± 39.8	Kv7.5	opener
Mibefradil	0.02± 0.0	0.00 ± 0.0	Cav1.2, Cav3.2	blocker
ICA-27243	0.20 ± 0.1	0.00 ± 0.0	Kv7.2/7.3	opener
ML213	0.38 ± 0.4	0.00 ± 0.0	Kv7.2/7.4	opener
SKA 31	106.67 ± 44.4	123.33 ± 60.8	KCa2	opener
CyPPA (NS6277)	12.72 ± 5.8	80.00 ± 27.4	SK2, SK3, KCa2.2/2.3	allosteric modulator
1-Ebio (SB-423901)	122.81 ± 27.8	103.33 ± 21.7	SK1, SK2, SK3, KCa2. 1/2.2/2.3	allosteric modulator
NS309	86.56 ± 14.4	110.00 ± 38.4	SK1, SK2, SK3, KCa2. 1/2.2/2.3	allosteric modulator
ICA 069673	0.07 ± 0.0	13.33 ± 13.9	Kv7.2/7.3	opener
Phenytoin	103.78 ± 41.1	116.67 ± 56.5	Nav1.1	blocker
Loperamide	0.02 ± 0.0	0.00± 0.0	CaV2.2	blocker

For the primary screen, 2,899 compounds from the CGL3 library were added at a concentration of 3 μM selected to obtain a balance between potency and off-target effects (Jones and Bunnage, 2017). The activity of individual neurons was recorded, and average spike rate per cell was calculated for each well to reduce variability, with an average Z' factor of 0.5 (Figure S2C; 5 μM TTX as positive control). Average spike rate per cell in each well was expressed as a ratio to DMSO controls, and the average percentage change in activity of two replicates was calculated for each time point (Figure 2B). We set cutoffs of −30% for defining decreased GCaMP activity (inhibition) and +30% for increased activity (excitation), a cutoff typically used for a medium-sized library. Compounds that increased or decreased GCaMP activities greater than or equal to cutoff at either 6 or 24 h were considered hits in the primary screen. Among the 2,899 compounds tested, 242 decreased GCaMP activity and 89 increased it, with most compounds showing similar effects at 6 and 24 h. The remaining 2,572 compounds in the library (89%) were below the two cutoffs (Figure 2C).

Confirmation GCaMP screen

Primary screen hit compounds (327) as well as a set of potential false negatives (76) were retested at 3 μM in a confirmation screen. The same assay and analysis as for the primary screen were used (Figure S2D). About one-third of the 401 compounds tested (two compounds were not available for reordering) were consistent between the primary and confirmation screen. Only 4 of the 76 potential false-negative compounds had activity above cutoff, indicating a low false-negative rate. In total, we found from the confirmation screen 84 compounds that decreased GCaMP activity and 22 that increased it (Figure S2E; Table S1). These compounds (26% hit confirmation rate) cover multiple different targets and entered the next step of the screening funnel.

Efficacy and toxicity dose-response assays

To exclude compounds that decreased excitability due to toxicity, we compared relative efficacy and toxicity for the 101 hit compounds (several compounds were duplicated or unavailable for reorder) at five concentrations: 0.024, 0.12, 0.6, 3, and 15 μM. The half-maximal inhibitory concentration (IC_{50}) values for decreasing GCaMP activity at 6 and 24 h were extrapolated from the generated dose-response curve. The IC_{50} for decreasing neuronal viability was calculated through a CellTiterGlo (CTG) assay that measures cellular ATP levels. Most compounds showed a dose-dependent effect on GCaMP activity without any indication of cytotoxicity at any dose, suggesting that these compounds decrease neuronal activity rather than affect viability (Figures 2D and 2G). However, a few compounds showed dose-dependent decreases in viability (Figures 2E, 2F, 2H, and 2I). We considered an $IC_{50} < 10$ μM for the GCaMP at either 6 or 24 h as effective and a >30-fold difference between the GCaMP IC_{50} and toxicity IC_{50} as non-toxic (Figure 2J). Among the 101 compounds tested, 20 had an $IC_{50} > 10$ μM and 14 were cytotoxic, leaving 67 compounds as effective ALS motor neuron hyperexcitability-reducing compounds (Figure 2K; Table S2).

Target deconvolution

Sixty-seven of the 2,899 compounds in the CGL3 library were identified by the three rounds of screening as effectively decreasing motor neuron calcium activity (2.3% hit rate) (Figure 3A). The entire library covers 1,043 different targets and the 67 hits covered 153 targets, including enzymes, GPCRs, ion channels, lipoproteins, transcription factors, and transporters (Figure 3B). Because most chemical compounds act on more than one target, it is difficult to deconvolute the true target from individual compounds. To detect with confidence which molecular targets change neuronal excitability, we performed a target enrichment analysis (Figure S3). For each of the 153 putative targets, we compared the number of respective compounds in the library annotated for the target before the screen and in the final list of 67 compounds after the screen, to decide whether multiple distinct compounds acting on the same target were enriched through the screen. This analysis revealed 13 putative targets: *GRIA1*, *GRIA2*, *GRIA3*, *GRIA4*, *KCNQ1*, *KCNQ2*, *KCNQ3*, *SCN5A*, *SCN10A*, *DRD3*, *HRH4*, *OPRK1*, and *SSTR5* (Figure 3C).

The activity of the 67 hit compounds was then tested by MEA (Figure 3D), and all the targets nominated by the enrichment analysis were confirmed to modulate neuronal excitability, again confirming that the primary GCaMP screen detected excitability changes (Table S3). Transcripts of the putative targets (*GRI1A1*, *GRIA2*, *GRIA3*, *GRIA4*, *KCNQ2*, and *KCNQ3*), or of close family members/isoforms of *KCNQ1*, *SCN5A*, *SCN10A*, *DRD3*, *HRH4*, and *SSTR5*, were abundantly expressed in human motor neurons, except for *OPRK1*, the kappa opioid receptor, supporting

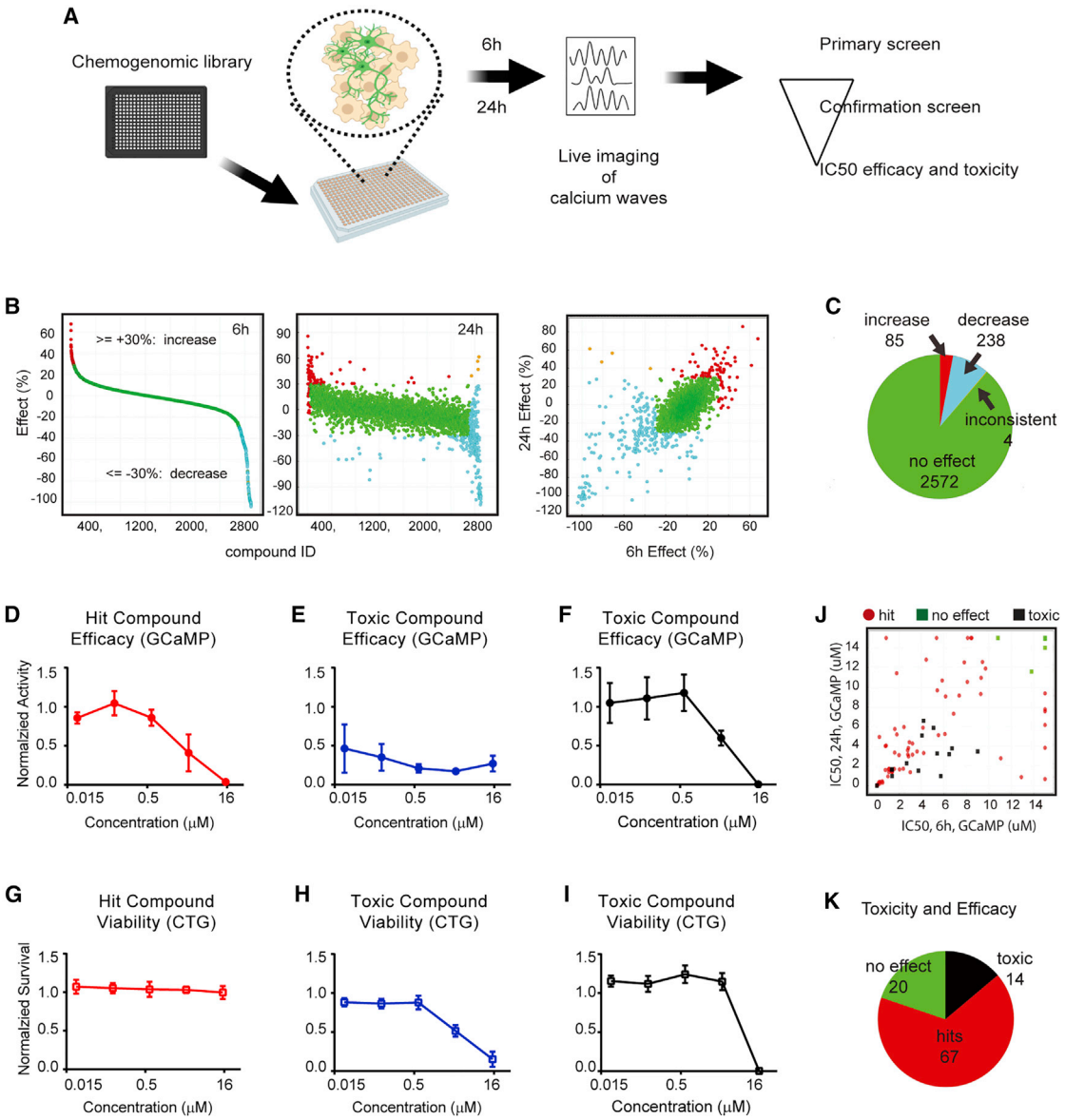

Figure 2. Phenotypic screen to identify compounds that decrease motor neuron excitability

(A) Screening scheme. ALS human motor neurons and mouse glia were cocultured in 384-well plates and infected by lenti-hsyn-GCaMP6s. Compounds from a chemogenomic library were added after 3–4 weeks, followed by GCaMP live imaging after 6 and 24 h.

(B and C) Primary GCaMP screen. (B) Compounds' effects on motor neuron excitability (n = 2, presented as average % effects, compared with DMSO). Compounds that increase/decrease greater than or equal to 30% GCaMP activities were considered hits. Red, increase; blue, decrease; green, no effect; orange, inconsistent between 6 and 24 h. (C) Results of primary screen.

(D–K) Toxicity and efficacy screen. Compounds selected from primary and confirmation screens were further tested to compare the dose-dependent effects on neuron viability (CTG assay) and activity (GCaMP assay). (D and G) Example of a hit compound. (E and H) Example from a toxic and ineffective compound. (F and I) Example from an effective, but toxic compound (n = 4, mean ± SD). (J) Compounds with a <10 μM activity IC_{50} and with a >30-fold difference between activity and toxicity. IC_{50} were validated hits. Red, hit; black, toxic; green, ineffective. (K) Results of toxicity and efficacy assays. See also Figure S2 and Tables S1 and S2.

that a bioinformatic deconvolution of hits based on their annotation likely revealed "true targets" that modulate neuronal excitability (GEO: GSE54409) (Figure 3E).

Target validation

Seven of the 13 targets belonged to two classes: AMPA receptors (*GRIA1*, *GRIA2*, *GRIA3*, and *GRIA4*) and Kv7 voltage-gated potassium channels (*KCNQ2* and *KCNQ3*). We confirmed that compounds annotated for these two classes can effectively decrease *SOD1(A4V)* motor neuron activities on MEA (Figure 4A; Table S3). Two Kv7.2/7.3 openers, retigabine and flupirtine, were found to block firing of human motor neurons carrying *SOD1*, *C9ORF72*, and *FUS* mutations in our previous study (Wainger et al., 2014), suggesting the action is not mutation dependent.

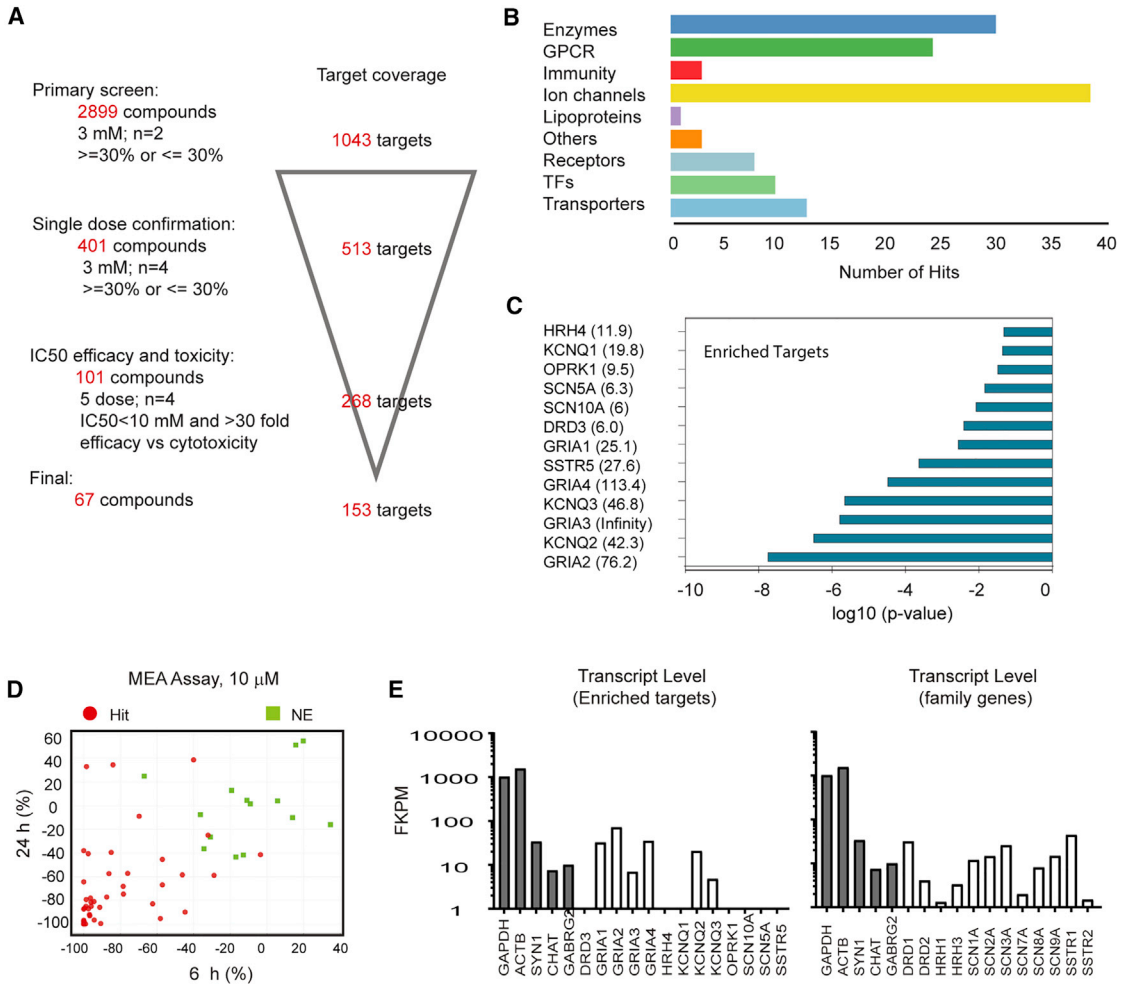

Figure 3. Target deconvolution and validation

(A) Summary of screening funnel. Sixty-seven compounds associated with 153 targets were identified through three rounds of screening from the initial 2,899 (2,882 distinct) compounds.

(B) Targets covered by the final 67 compounds.

(C) Thirteen bioinformatically enriched targets. The number in parentheses shows the enrichment factor of each target.

(D) MEA validation of the final 67 compounds. *SOD1(A4V)* motor neurons were cultured with glia for 3–4 weeks, and the effects of compounds (10 μM) were measured 6 and 24 h after compound addition. Compounds' effects were normalized to baseline activities (before the treatment) and compared with the DMSO control. Red, hit compound; green, ineffective compound.

(E) Transcript levels of enriched targets and associated family members in *SOD1(A4V)* motor neurons. See also Figure S3 and Table S3.

Retigabine also decreased lower motor neuron hyperexcitability in two recent clinical trials on patients with ALS (Kovalchuk et al., 2018; Wainger et al., 2021), validating the action of Kv7 channels in controlling human motor neuron hyperexcitability in patients. AMPA receptors are glutamate-gated cation channels whose calcium permeability is subject to both posttranscriptional and posttranslational modifications (Weiss, 2011). We found that AMPA elicits a large calcium influx in differentiated human ALS motor neurons by fura-2 imaging (Figure 4B) and increases firing in MEA recordings (Figure S4A), confirming AMPA receptor activity.

To examine whether the phenotypic screen identified targets that have not been associated with motor neuron excitability, we compared the enriched targets (Figure 3C) with the compound's annotation (Table S3) and found DRD3 as a promising putative target. DRD3 encodes the D3 subtype of the 5 dopamine-gated GPCRs that participate in multiple neurological activities (Bozzi and Borrelli, 2006; Beaulieu and Gainetdinov, 2011). Although DRD3 transcripts are expressed at low levels in ALS motor neurons (Figure 3E), its close family member DRD2 is expressed in both differentiated motor neurons (Figure 3E) and the human spinal cord (D'Erchia et al., 2017). More importantly, all active compounds in the CGL3 library annotated for DRD3 also have activity on DRD2 (Table S3). We therefore wondered whether it was the DRD2 and not the DRD3 receptor that modulates ALS motor neuron hyperexcitability. CGL3 library compounds that target DRD2/3 efficiently decreased *SOD1(A4V)* motor neuron firing in MEA (Figure 4A). We also tested

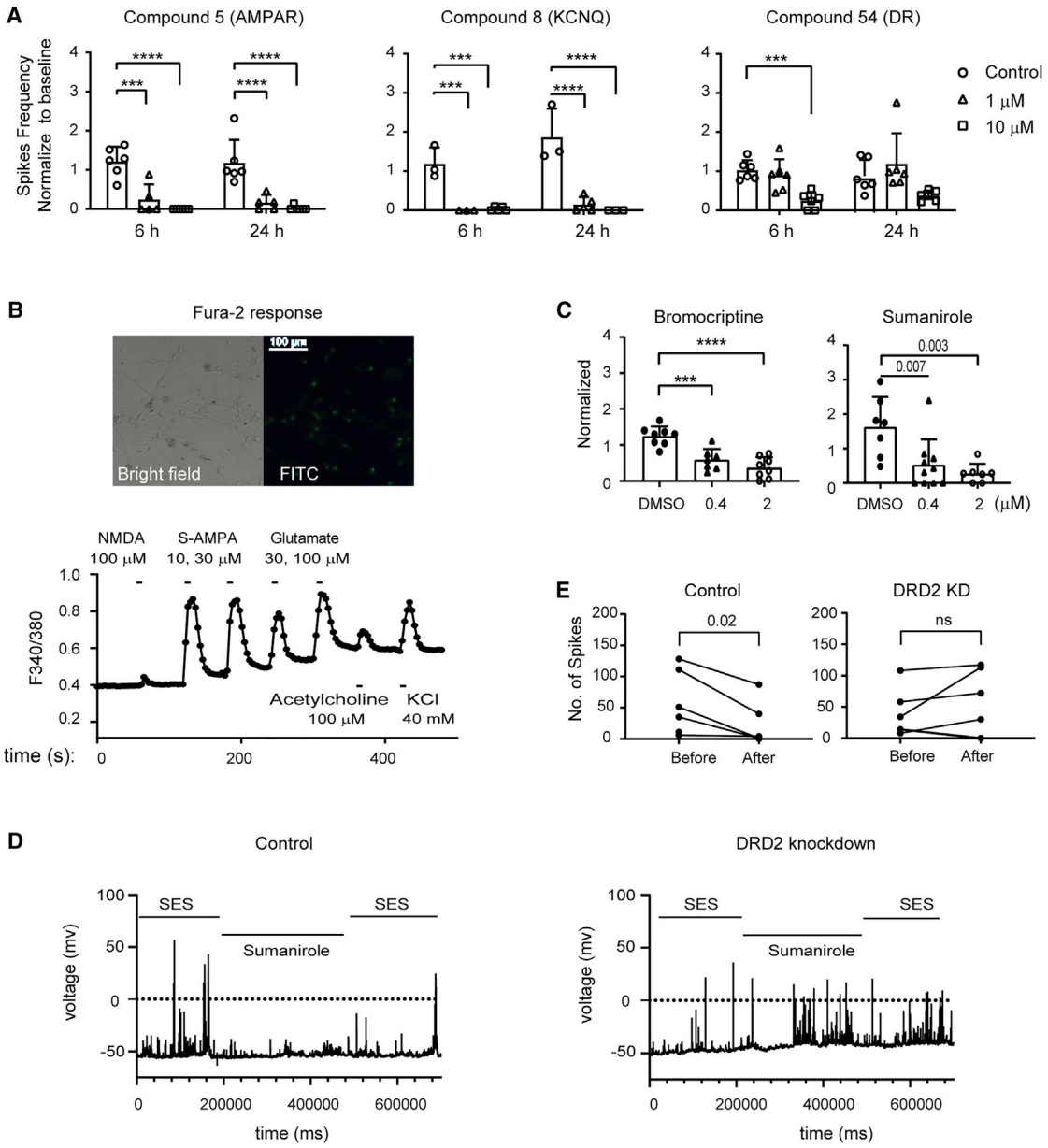

Figure 4. Target validation

(A) Effect of CGL3 library compounds acting on AMPA receptor, KCNQ/Kv7.2/3, and dopamine receptor on *SOD1(A4V)* motor neuron excitability tested by MEA. Six or 24 h after compound addition, neuronal activities were measured and normalized to activity before the treatment. (n = 3–6 wells, mean ± SD, one-way ANOVA followed by Dunnett's multiple comparisons test).

(B) AMPA-induced calcium influx tested by fura-2 imaging. Motor neuron-glia cocultures loaded with fura-2 dye and neurons with big soma (left, differential interference contrast [DIC]) and bright fura-2 signal (right, 380 nM, fluorescein isothiocyanate [FITC]) were selected for analysis (n = 4 individual assays; scale bar, 100 μm).

(C) DRD2 agonist effects on *SOD1(A4V)* motor neurons (n = 7–10 wells, mean ± SD, one-way ANOVA followed by Dunnett's multiple comparisons test).

(D) Effects of the DRD2 agonist sumanirole on *SOD1(A4V)* motor neurons with and without DRD2 knockdown, tested by current-clamp recording. Membrane potentials were held at ~–50 mV, and compounds were perfused for 300 s and then washed off by standard extracellular solution (SES).

(E) Summary of current-clamp recordings. Action potential spikes showing a peak amplitude above 0 mV were calculated from control (GFP knockdown) and DRD2 knockdown motor neurons 0–100 s before and 100–200 s after sumanirole (10 μM) perfusion. ***$p \leq 0.001$; ****$p < 0.0001$. See also Figure S4.

other commercially available DRD2/3 agonists, including bromocriptine, a potent but non-specific agonist, and sumanirole, a highly selective and potent DRD2 agonist (Ki = 2 versus 1,940 nM for DRD2 versus DRD3) (McCall et al., 2005), and both compounds decreased *SOD1(A4V)* motor neuron excitability (Figure 4C). Sumanirole also decreased activity of control

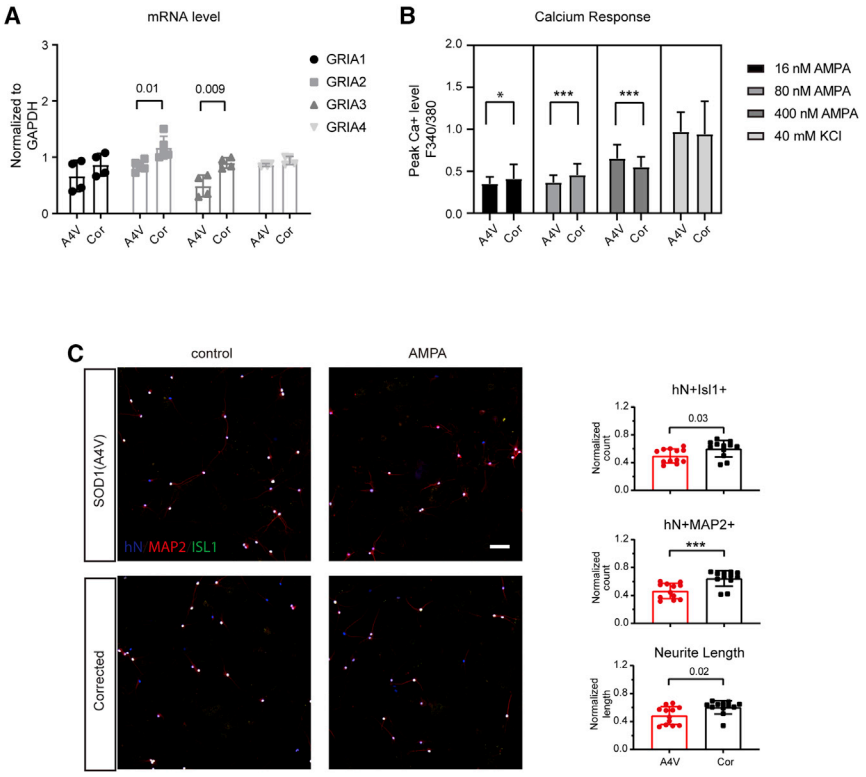

Figure 5. AMPA toxicity in ALS

(A) AMPA receptor subunit expression in *SOD1(A4V)* motor neurons and corrected isogenic controls (n = 4–5 samples, mean ± SD, two-tailed t test).

(B) AMPA-induced calcium influx peak tested by fura-2 imaging (n = 50–70 neurons, mean ± SD, two-tailed t test, df = 135).

(C) AMPA toxicity. AMPA (50 μM) and cyclothiazide (10 μM) were added to the culture for 48 h and then cells were fixed and stained with human nucleus (hN), MAP2, and the motor neuron marker Islet-1 (Isl1). The number of hN^+Isl1^+ nuclei, hN^+MAP2^+ neurons, and the total length of $MAP2^+$ neurites (μm) per well were measured and normalized to untreated condition of each genotype (n = 12 wells, mean ± SD, two-tailed t test; scale bar, 100 μm). *p ≤ 0.05; **p ≤ 0.01; ***p ≤ 0.001. See also Figure S5.

motor neurons (Figure S4B), with greater effects at 6 h than at 24 h, suggesting possible receptor desensitization. We also examined the effects of sumanirole by patch clamp and observed a decrease in firing frequency (Figure 4D). The decrease in neuronal firing produced by sumanirole was slow in onset and accompanied by a slight hyperpolarization, while recovery after wash was also slow, as expected for a GPCR-mediated secondary signaling pathway. To confirm that sumanirole's effects on excitability were due to an action on DRD2, we applied sumanirole to motor neurons subject to short hairpin RNA (shRNA)-mediated DRD2 knockdown. In contrast to control neurons, DRD2 knockdown motor neurons were insensitive to sumanirole treatment in terms of reduced excitability (Figures 4D and 4E). A further examination of the effect of sumanirole on ALS motor neurons with *C9ORF72* expansion (Figure S4C) revealed that DRD2 modulates motor neuron excitability independent of a specific mutation.

Excitability and motor neuron survival

We have shown previously that steady-state potassium currents are reduced in ALS motor neurons and that increasing Kv7.2/3 activity rescues ALS motor neurons from both hyperexcitability and cell death (Wainger et al., 2014). We now studied the potential role of the two other excitability modulators, AMPA receptors and DRD2, in ALS disease pathogenesis. We first compared the transcript level of AMPA receptors and interestingly found decreased expression of GRIA2 and GRIA3 in the *SOD1(A4V)* motor neurons (Figure 5A). AMPA receptors are homo- or hetero-tetramers composed by different subunits, and the exclusion of GRIA2 increases calcium permeability (Weiss, 2011), which may increase AMPA excitotoxicity. To test this, we first studied AMPA-induced calcium influx by fura-2 imaging (Figure 5B). Although there was no difference in total voltage-dependent calcium influx, as measured by KCl-evoked responses, *SOD1(A4V)* patient motor neurons exhibited an altered calcium influx to AMPA compared with the isogenic control, with smaller responses at low concentrations (16 and 80 nM) and a larger response at a higher concentration (400 nM), suggesting that AMPA receptor subcomposition on the membrane may be different between disease and control motor neurons. We also compared AMPA-induced excitotoxicity and found that patient-derived neurons showed increased sensitivity to cell death on exposure to 50 μM AMPA compared with the isogenic controls (Figure 5C). Therefore, AMPA receptors, as revealed by our hyperexcitability phenotypic screen, may contribute to the increased vulnerability to cell death of ALS motor neurons. Whether this resulted from altered AMPA receptor activity, or other factors such as reactive oxygen species (ROS) clearance defects, requires future examination.

Although DRD2 transcript levels did not differ between the *SOD1(A4V)* and isogenic control motor neurons (Figure S5A), suggesting that the receptor is not a driver of disease pathophysiology, we found that shRNA knockdown of DRD2 increased cell death (Figure S5B), which together with earlier reports that DRD2 agonists attenuate ALS phenotypes (Fujimori et al., 2018; Nagata et al., 2016) suggests that DRD2 agonism may increase motor neuron survival and that this may be a potential disease-modifying target.

DISCUSSION

Target-based screens are ideal for discovering compounds with high potency and selectivity for a specific protein. By contrast, phenotypic screens open the opportunity to discover, in an unbiased fashion, novel targets/mechanisms related to specific

aspects of disease pathogenesis or modification in human cells and provide validation for known targets. While most published screens related to ALS focus on survival and neurite outgrowth (Imamura et al., 2017; Yang et al., 2013; Sherman and Bang, 2018), we developed a screening strategy targeting abnormal electrophysiological properties to reveal targets that modulate the intrinsic hyperexcitability of ALS motor neurons (Figure 1).

Neuronal hyperexcitability is a common pathologic event in both spinal motor and cortical neurons of patients with ALS. In patients, transcranial magnetic stimulation of the motor cortex has revealed that cortical hyperexcitability is a feature in the early phase of the disease (Geevasinga et al., 2016; Shibuya et al., 2016), while threshold tracking in peripheral nerve recordings indicates that intrinsic motor axonal hyperexcitability is a predictor of shorter patient survival (Kanai et al., 2012). Increased axonal excitability reflects aberrant sodium and potassium currents in motor neurons and could be a contributor to motor neuron degeneration in patients (Park et al., 2017). In some rodent ALS models, hyperexcitability manifests as alterations in sodium currents, neurotransmission, and calcium homeostasis (Pieri et al., 2003; Kuo et al., 2005; van Zundert et al., 2008; Kim et al., 2017). Brain slice recordings from neonatal mice overexpressing SOD1(G93A) protein reveal increased intrinsic membrane excitability and persistent sodium currents, suggesting that hyperexcitability presents before pathological degeneration. However, some studies in mouse models find that motor neurons are not hyperexcitable and in some cases are hypoexcitable (Leroy et al., 2014; Delestrée et al., 2014; Martínez-Silva et al., 2018) and have even suggested that neuronal hyperexcitability may be protective (Saxena et al., 2013). These discrepancies are probably due to differences in the disease stage (embryonic, neonatal, pre-symptomatic, symptomatic, and late in the disease), the specific aspects of neuronal excitability that were measured (spontaneous action potential firing, membrane potential, response to current injections, and channel activities) and the method used (intra- or extracellular recordings from cultured cells, slices or from an animal model). Importantly, while in some studies motor neurons that lose repetitive firing have been characterized as hypoexcitable, the neurons exhibit depolarized membrane potentials, which leads to an inactivation of sodium channels that blocks action potential firing (Martínez-Silva et al., 2018; Devlin et al., 2015); therefore, this "hypoexcitability" is actually a manifestation of overexcitation/membrane depolarization. A recent report also suggests that the "hypoexcitability" in the SOD1(G93A) transgenic mice observed *in vivo* is actually the consequence of incorrect techniques utilized in the studies, and by using more appropriate technology, these authors actually found hyperexcitability in the mutant motor neurons (Jensen et al., 2020), as is present both in human patients and patient-derived motor neurons. This strongly suggests that the hyperexcitability phenotype is a major and robust feature of ALS and that hypoexcitability may in some cases be an artifact.

Neuronal hyperexcitability is also observed in other neurological disorders such as Alzheimer's disease (Šišková et al., 2014) and Huntington's disease (Cao et al., 2015) and causes TDP43 (TAR DNA binding protein 43) pathology in human iPSC-derived neurons (Weskamp et al., 2020). Decreasing the excitability of cortical pyramidal neurons delays disease onset in SOD1(G93A) mice, indicating that blocking neuronal hyperexcitability can be beneficial (Khademullah et al., 2020). A recent study has shown that *C9orf72* knockout rats have no motor neuron degeneration, but they have increased sensitivity to excitotoxicity of motor neurons (Dong et al., 2021), suggesting that disease progression may result from interaction of mutations that increase vulnerability and a trigger or stressor and the excitation may be the latter. Therapeutic intervention may need to target both.

The combination of the clinical hyperexcitability data (Park et al., 2017; Wainger et al., 2021), the excitability increases in rodent models (Jensen et al., 2020), and in iPSC-derived motor neurons from patients with ALS (Wainger et al., 2014) suggests that hyperexcitability is a robust ALS phenotype, in at least a large subset of patients. Our aim here was to develop a screening platform to identify molecular targets modulating hyperexcitability as the first step for exploring novel therapeutic strategies. Using live single-cell GCaMP imaging, we were able to monitor neuronal activity in a high-throughput format, one that offered technical advantages over patch-clamp and MEA recordings, with a Z' factor of 0.5. While sacrificing the temporal resolution of directly recording neuronal activity, we could nevertheless evaluate >300 compounds within a few hours. Through three rounds of successive GCaMP screens (Figure 3A), we identified 67 compounds from a 2,899-compound chemogenomic library that decreased ALS motor neuron hyperexcitability effectively without cytotoxicity. Enrichment analysis revealed thirteen individual potential targets and of these two, AMPA receptors and the Kv7 channels, are already known to produce hyperexcitability and our data further validate this role. In addition, we revealed that DRD2 receptor agonists also modulate motor neuron hyperexcitability, making it a target for such disease-modifying action.

AMPA receptors are glutamate-gated ion channels and aberrant glutamatergic neurotransmission is present in both mouse models and patients with ALS (King et al., 2016). AMPA receptor antagonists rescue TDP43 pathology in a rodent ALS model (Akamatsu et al., 2016) and the Food and Drug Administration (FDA)-approved drug riluzole may protect against motor neuron death by inhibiting glutamatergic neurotransmission (Jin et al., 2010), although the drug also has action on several other targets including sodium channels. In motor neurons carrying the *C9ORF72* expansion, expression of calcium-permeable AMPA receptor subtypes increases vulnerability to glutamate-mediated excitotoxicity (Selvaraj et al., 2018; Shi et al., 2018). In this study, we also show that SOD1 ALS motor neurons are more vulnerable to AMPA-induced cell death, suggesting that the AMPA receptor could be a common target for treating ALS arising from different genetic origins (Figure 5). Perampanel, an AMPA receptor antagonist, is currently being evaluated in a clinical trial for its effects on ALS progression (ClinicalTrials.gov Identifier: NCT03377309). Similar to a recent study on SOD1(G93A) mice (Bączyk et al., 2020), we also observed altered expression of AMPA receptor subunits. Nevertheless, whether it results from, or leads to, increased AMPA toxicity, and how it is related to other ALS pathologies, requires further study.

The other enriched target family detected by the screen, voltage-dependent Kv7 potassium channels, plays an important

role in controlling neuronal excitability. Activation of Kv7 channels prevents repetitive firing, and loss-of-function mutations are linked to genetic epilepsy (Greene and Hoshi, 2017). In an earlier study, we identified decreased potassium currents in differentiated motor neurons carrying the *SOD1(A4V)* mutation compared with isogenic control neurons and an increase in spikes generated in response to current injection by patch clamp, which was reduced by the activation of Kv7, which also rescued motor neuron survival (Wainger et al., 2014). Here, we independently and in an unbiased manner, confirm that Kv7 channels are important modulators of ALS motor neuron excitability. A clinical trial recently revealed the efficacy of the Kv7 channel opener retigabine in reducing hyperexcitability in patients with ALS measured by a biomarker linked to patient survival (Kovalchuk et al., 2018), which supports that the phenotypic approach can identify clinically meaningful targets. Another larger phase 2a biomarker trial with 65 patients with ALS confirmed a dose-dependent effect of retigabine on two excitability biomarkers linked to patient survival and also found a significant correlation of the drug effect with compound muscle action potential (CMAP) amplitude, a marker for disease progression (Wainger et al., 2021). Additional long-duration clinical studies to assess the impact of Kv7.2/3 openers on disease progression will inform whether hyperexcitability is a major pathophysiological feature of ALS.

The DRD2 dopamine receptor is another excitability-modulating target identified by the screen, and its role in motor neurons is not clear. Both DRD2 and DRD3 belong to the type 2 dopamine receptor family, whose activation increases calcium signaling and potassium efflux (Beaulieu and Gainetdinov, 2011) and regulates autophagy (Wang et al., 2018). We did not observe altered DRD2 expression, suggesting it is not directly involved during ALS pathogenesis. Previously DRD2 agonists were shown to protect cortical and mesencephalic neurons from excitotoxicity (Sawada et al., 1998; Kihara et al., 2002). The agonists also decrease protein aggregation, increase neurite outgrowth, and prevent cell death in multiple ALS motor neuron lines through both dopamine-receptor-dependent and -independent pathways (Fujimori et al., 2018). Bromocriptine, a DRD2 agonist, sustained motor function in patients with ALS in a small-scale clinical trial (Nagata et al., 2016). We now show for the first time that DRD2 agonists modulate human motor neuron excitability, raising the possibility that this is one of the mechanisms of these agonists' action in ALS and that DRD2 could be used to modulate any hyperexcitability-driven component of disease progression. Our data do not support a role as a disease-causing target since its expression was not altered in patient motor neurons, but rather as a disease-modifying target. The screen will capture both sorts of targets.

There are some limitations to the approach utilized here. First, chemogenomic libraries are not without challenges: compound annotations are limited by the breadth/scope of the assay targets against which they have been tested and libraries may contain compounds enriched for common pharmacological targets such as GPCRs or kinases, and there is not equal representation of all target classes. Several of our enriched targets, such as DRD3, showed low transcript expression in motor neurons, while close family genes such as DRD2 were more abundantly expressed. This suggests incomplete annotation of the compounds in the CGL3 library, as most of them are based on *in vitro* assays using non-neuronal cells and thus the actual targets may be related family members/isoforms rather than the target suggested by the annotations. It may, in consequence, be worth grouping targets with similar pharmacological properties together for target deconvolution and then separately identifying the specific target involved by genetic manipulation, such as shRNA knockdown, as we did here for DRD2.

ALS is a severe and typically fatal motor neuron disorder and patients urgently need effective therapies. Excitability phenotypic screening using patient-derived motor neurons is a novel and powerful method for the identification of drug targets that act on abnormal excitability. Validation of known targets highlights their potential involvement in ALS and should encourage consideration for drug development programs. The discovery of an involvement of DRD2 opens questions as to the source of dopamine in the ventral horn; its physiological role on motor neurons in healthy individuals; and most importantly, its potential disease-modifying role in ALS.

Live human-diseased neuronal excitability phenotypic screens are, we conclude, a powerful platform for the identification of disease-relevant and pharmacologically tractable drug targets, one that can be applied to the many neurological diseases characterized by abnormal excitability.

STAR★METHODS

Detailed methods are provided in the online version of this paper and include the following:

- KEY RESOURCES TABLE
- RESOURCE AVAILABILITY
  - Lead contact
  - Materials availability
  - Data and code availability
- EXPERIMENTAL MODEL AND SUBJECT DETAILS
  - Motor neuron differentiation and maintenance
  - Motoneuron-glial cocultures
- METHOD DETAILS
  - Magnetic cell sorting
  - Pfizer chemogenomic library
  - GCaMP live imaging
  - RNA knockdown
  - RT-qPCR
  - Toxicity assay (CellTiterGlo)
  - IC_{50} calculation
  - Multiple electrode array analysis
  - Enrichment analysis
  - Immunocytochemistry
  - Patch clamp recording
  - Calcium response imaging
- QUANTIFICATION AND STATISTICAL ANALYSIS

SUPPLEMENTAL INFORMATION

Supplemental information can be found online at https://doi.org/10.1016/j.celrep.2021.109224.

ACKNOWLEDGMENTS

This work was supported by funding from Target ALS and Pfizer CTI to C.J.W. and an ALSA Milton Safenowitz postdoctoral fellowship to K.C.D.R. NIH grant U54HD090255 supported the IDDRC screening core used at Boston Children's Hospital and 1R35NS105076 supported C.J.W. Dr. Giovanni Coppola from UCLA kindly provided us with the patient iPSC line carrying *C9ORF72* expansions. Dr. Elisabeth Engle from Boston Children's Hospital kindly provided the lenti-hsyn-GCaMP6s construct.

AUTHOR CONTRIBUTIONS

X.H., K.C.D.R., A.B., A.P.B., A.B.J., K.L.L., F.V., H.Y., A.J.C., K.E., L.H.J., and C.J.W. designed the research. X.H., K.C.D.R., O.W., K.C., D.F., R.M., A.G., M.K.D., M.T.S., and D.Z. performed the experiments. X.H., K.C.D.R., L.Z., A.B., A.P.B., A.B.J., J.K.M., H.Y., J.R.K., and S.L. analyzed the data. A.B.J., K.L.L., H.Y., and C.J.W. oversaw the project. X.H., K.R., and C.J.W. wrote the manuscript, with the help from the other authors.

DECLARATION OF INTERESTS

The authors declare the following competing financial interests: K.C.D.R., K.E., and C.J.W. are founders of QurAlis; L.Z., A.B., A.P.B., A.B.J., J.K.M., K.L.L., F.V., H.Y., L.H.J., and A.J.C. are current or previous employees of Pfizer.

Received: April 28, 2020
Revised: October 14, 2020
Accepted: May 13, 2021
Published: June 8, 2021

REFERENCES

Akamatsu, M., Yamashita, T., Hirose, N., Teramoto, S., and Kwak, S. (2016). The AMPA receptor antagonist perampanel robustly rescues amyotrophic lateral sclerosis (ALS) pathology in sporadic ALS model mice. Sci. Rep. *6*, 28649.

Bączyk, M., Alami, N.O., Delestrée, N., Martinot, C., Tang, L., Commisso, B., Bayer, D., Doisne, N., Frankel, W., Manuel, M., et al. (2020). Synaptic restoration by cAMP/PKA drives activity-dependent neuroprotection to motoneurons in ALS. J. Exp. Med. *217*, e20191734.

Beaulieu, J.M., and Gainetdinov, R.R. (2011). The physiology, signaling, and pharmacology of dopamine receptors. Pharmacol. Rev. *63*, 182–217.

Bilican, B., Serio, A., Barmada, S.J., Nishimura, A.L., Sullivan, G.J., Carrasco, M., Phatnani, H.P., Puddifoot, C.A., Story, D., Fletcher, J., et al. (2012). Mutant induced pluripotent stem cell lines recapitulate aspects of TDP-43 proteinopathies and reveal cell-specific vulnerability. Proc. Natl. Acad. Sci. USA *109*, 5803–5808.

Bozzi, Y., and Borrelli, E. (2006). Dopamine in neurotoxicity and neuroprotection: what do D2 receptors have to do with it? Trends Neurosci. *29*, 167–174.

Cao, Y., Bartolomé-Martín, D., Rotem, N., Rozas, C., Dellal, S.S., Chacon, M.A., Kadriu, B., Gulinello, M., Khodakhah, K., and Faber, D.S. (2015). Rescue of homeostatic regulation of striatal excitability and locomotor activity in a mouse model of Huntington's disease. Proc. Natl. Acad. Sci. USA *112*, 2239–2244.

Chen, Q., Cichon, J., Wang, W., Qiu, L., Lee, S.J., Campbell, N.R., Destefino, N., Goard, M.J., Fu, Z., Yasuda, R., et al. (2012). Imaging neural activity using Thy1-GCaMP transgenic mice. Neuron *76*, 297–308.

Chen, T.W., Wardill, T.J., Sun, Y., Pulver, S.R., Renninger, S.L., Baohan, A., Schreiter, E.R., Kerr, R.A., Orger, M.B., Jayaraman, V., et al. (2013). Ultrasensitive fluorescent proteins for imaging neuronal activity. Nature *499*, 295–300.

Cong, F., Cheung, A.K., and Huang, S.M. (2012). Chemical genetics-based target identification in drug discovery. Annu. Rev. Pharmacol. Toxicol. *52*, 57–78.

Delestrée, N., Manuel, M., Iglesias, C., Elbasiouny, S.M., Heckman, C.J., and Zytnicki, D. (2014). Adult spinal motoneurones are not hyperexcitable in a mouse model of inherited amyotrophic lateral sclerosis. J. Physiol. *592*, 1687–1703.

D'Erchia, A.M., Gallo, A., Manzari, C., Raho, S., Horner, D.S., Chiara, M., Valletti, A., Aiello, I., Mastropasqua, F., Ciaccia, L., et al. (2017). Massive transcriptome sequencing of human spinal cord tissues provides new insights into motor neuron degeneration in ALS. Sci. Rep. *7*, 10046.

Devlin, A.C., Burr, K., Borooah, S., Foster, J.D., Cleary, E.M., Geti, I., Vallier, L., Shaw, C.E., Chandran, S., and Miles, G.B. (2015). Human iPSC-derived motoneurons harbouring TARDBP or C9ORF72 ALS mutations are dysfunctional despite maintaining viability. Nat. Commun. *6*, 5999.

Di Giorgio, F.P., Boulting, G.L., Bobrowicz, S., and Eggan, K.C. (2008). Human embryonic stem cell-derived motor neurons are sensitive to the toxic effect of glial cells carrying an ALS-causing mutation. Cell Stem Cell *3*, 637–648.

Dong, W., Ma, Y., Guan, F., Zhang, X., Chen, W., Zhang, L., and Zhang, L. (2021). Ablation of C9orf72 together with excitotoxicity induces ALS in rats. FEBS J. *288*, 1712–1723.

Donnelly, C.J., Zhang, P.W., Pham, J.T., Haeusler, A.R., Mistry, N.A., Vidensky, S., Daley, E.L., Poth, E.M., Hoover, B., Fines, D.M., et al. (2013). RNA toxicity from the ALS/FTD C9ORF72 expansion is mitigated by antisense intervention. Neuron *80*, 415–428.

Fujimori, K., Ishikawa, M., Otomo, A., Atsuta, N., Nakamura, R., Akiyama, T., Hadano, S., Aoki, M., Saya, H., Sobue, G., and Okano, H. (2018). Modeling sporadic ALS in iPSC-derived motor neurons identifies a potential therapeutic agent. Nat. Med. *24*, 1579–1589.

Geevasinga, N., Menon, P., Özdinler, P.H., Kiernan, M.C., and Vucic, S. (2016). Pathophysiological and diagnostic implications of cortical dysfunction in ALS. Nat. Rev. Neurol. *12*, 651–661.

Greene, D.L., and Hoshi, N. (2017). Modulation of Kv7 channels and excitability in the brain. Cell. Mol. Life Sci. *74*, 495–508.

Imamura, K., Izumi, Y., Watanabe, A., Tsukita, K., Woltjen, K., Yamamoto, T., Hotta, A., Kondo, T., Kitaoka, S., Ohta, A., et al. (2017). The Src/c-Abl pathway is a potential therapeutic target in amyotrophic lateral sclerosis. Sci. Transl. Med. *9*, eaaf3962.

Iwai, Y., Shibuya, K., Misawa, S., Sekiguchi, Y., Watanabe, K., Amino, H., and Kuwabara, S. (2016). Axonal Dysfunction Precedes Motor Neuronal Death in Amyotrophic Lateral Sclerosis. PLoS ONE *11*, e0158596.

Jensen, D.B., Kadlecova, M., Allodi, I., and Meehan, C.F. (2020). Spinal motoneurones are intrinsically more responsive in the adult G93A SOD1 mouse model of amyotrophic lateral sclerosis. J. Physiol. *598*, 4385–4403.

Jin, L.J., Schlesinger, F., Song, Y.P., Dengler, R., and Krampfl, K. (2010). The interaction of the neuroprotective compounds riluzole and phenobarbital with AMPA-type glutamate receptors: a patch-clamp study. Pharmacology *85*, 54–62.

Jones, L.H., and Bunnage, M.E. (2017). Applications of chemogenomic library screening in drug discovery. Nat. Rev. Drug Discov. *16*, 285–296.

Kanai, K., Shibuya, K., Sato, Y., Misawa, S., Nasu, S., Sekiguchi, Y., Mitsuma, S., Isose, S., Fujimaki, Y., Ohmori, S., et al. (2012). Motor axonal excitability properties are strong predictors for survival in amyotrophic lateral sclerosis. J. Neurol. Neurosurg. Psychiatry *83*, 734–738.

Kanning, K.C., Kaplan, A., and Henderson, C.E. (2010). Motor neuron diversity in development and disease. Annu. Rev. Neurosci. *33*, 409–440.

Khademullah, C.S., Aqrabawi, A.J., Place, K.M., Dargaei, Z., Liang, X., Pressey, J.C., Bedard, S., Yang, J.W., Garand, D., Keramidis, I., et al. (2020). Cortical interneuron-mediated inhibition delays the onset of amyotrophic lateral sclerosis. Brain *143*, 800–810.

Kihara, T., Shimohama, S., Sawada, H., Honda, K., Nakamizo, T., Kanki, R., Yamashita, H., and Akaike, A. (2002). Protective effect of dopamine D2 agonists in cortical neurons via the phosphatidylinositol 3 kinase cascade. J. Neurosci. Res. *70*, 274–282.

Kim, J., Hughes, E.G., Shetty, A.S., Arlotta, P., Goff, L.A., Bergles, D.E., and Brown, S.P. (2017). Changes in the Excitability of Neocortical Neurons in a Mouse Model of Amyotrophic Lateral Sclerosis Are Not Specific to

Corticospinal Neurons and Are Modulated by Advancing Disease. J. Neurosci. *37*, 9037–9053.

King, A.E., Woodhouse, A., Kirkcaldie, M.T., and Vickers, J.C. (2016). Excitotoxicity in ALS: Overstimulation, or overreaction? Exp. Neurol. *275*, 162–171.

Kiskinis, E., Sandoe, J., Williams, L.A., Boulting, G.L., Moccia, R., Wainger, B.J., Han, S., Peng, T., Thams, S., Mikkilineni, S., et al. (2014). Pathways disrupted in human ALS motor neurons identified through genetic correction of mutant SOD1. Cell Stem Cell *14*, 781–795.

Klim, J.R., Williams, L.A., Limone, F., Guerra San Juan, I., Davis-Dusenbery, B.N., Mordes, D.A., Burberry, A., Steinbaugh, M.J., Gamage, K.K., Kirchner, R., et al. (2019). ALS-implicated protein TDP-43 sustains levels of STMN2, a mediator of motor neuron growth and repair. Nat. Neurosci. *22*, 167–179.

Kovalchuk, M.O., Heuberger, J.A.A.C., Sleutjes, B.T.H.M., Ziagkos, D., van den Berg, L.H., Ferguson, T.A., Franssen, H., and Groeneveld, G.J. (2018). Acute Effects of Riluzole and Retigabine on Axonal Excitability in Patients With Amyotrophic Lateral Sclerosis: A Randomized, Double-Blind, Placebo-Controlled, Crossover Trial. Clin. Pharmacol. Ther. *104*, 1136–1145.

Kuo, J.J., Siddique, T., Fu, R., and Heckman, C.J. (2005). Increased persistent Na(+) current and its effect on excitability in motoneurones cultured from mutant SOD1 mice. J. Physiol. *563*, 843–854.

Leroy, F., Lamotte d'Incamps, B., Imhoff-Manuel, R.D., and Zytnicki, D. (2014). Early intrinsic hyperexcitability does not contribute to motoneuron degeneration in amyotrophic lateral sclerosis. eLife *3*, 3.

Lopez-Gonzalez, R., Lu, Y., Gendron, T.F., Karydas, A., Tran, H., Yang, D., Petrucelli, L., Miller, B.L., Almeida, S., and Gao, F.B. (2016). Poly(GR) in C9ORF72-Related ALS/FTD Compromises Mitochondrial Function and Increases Oxidative Stress and DNA Damage in iPSC-Derived Motor Neurons. Neuron *92*, 383–391.

Martínez-Silva, M.L., Imhoff-Manuel, R.D., Sharma, A., Heckman, C.J., Shneider, N.A., Roselli, F., Zytnicki, D., and Manuel, M. (2018). Hypoexcitability precedes denervation in the large fast-contracting motor units in two unrelated mouse models of ALS. eLife *7*, e04046.

McCall, R.B., Lookingland, K.J., Bédard, P.J., and Huff, R.M. (2005). Sumanirole, a highly dopamine D2-selective receptor agonist: in vitro and in vivo pharmacological characterization and efficacy in animal models of Parkinson's disease. J. Pharmacol. Exp. Ther. *314*, 1248–1256.

Nagata, E., Ogino, M., Iwamoto, K., Kitagawa, Y., Iwasaki, Y., Yoshii, F., Ikeda, J.E., and Investigators, A.L.S.C.; ALS Consortium Investigators (2016). Bromocriptine Mesylate Attenuates Amyotrophic Lateral Sclerosis: A Phase 2a, Randomized, Double-Blind, Placebo-Controlled Research in Japanese Patients. PLoS ONE *11*, e0149509.

Nakata, M., Kuwabara, S., Kanai, K., Misawa, S., Tamura, N., Sawai, S., Hattori, T., and Bostock, H. (2006). Distal excitability changes in motor axons in amyotrophic lateral sclerosis. Clin. Neurophysiol. *117*, 1444–1448.

Park, S.B., Kiernan, M.C., and Vucic, S. (2017). Axonal Excitability in Amyotrophic Lateral Sclerosis : Axonal Excitability in ALS. Neurotherapeutics *14*, 78–90.

Pieri, M., Albo, F., Gaetti, C., Spalloni, A., Bengtson, C.P., Longone, P., Cavalcanti, S., and Zona, C. (2003). Altered excitability of motor neurons in a transgenic mouse model of familial amyotrophic lateral sclerosis. Neurosci. Lett. *351*, 153–156.

Robberecht, W., and Philips, T. (2013). The changing scene of amyotrophic lateral sclerosis. Nat. Rev. Neurosci. *14*, 248–264.

Sancak, Y., Peterson, T.R., Shaul, Y.D., Lindquist, R.A., Thoreen, C.C., Bar-Peled, L., and Sabatini, D.M. (2008). The Rag GTPases bind raptor and mediate amino acid signaling to mTORC1. Science *320*, 1496–1501.

Sawada, H., Ibi, M., Kihara, T., Urushitani, M., Akaike, A., Kimura, J., and Shimohama, S. (1998). Dopamine D2-type agonists protect mesencephalic neurons from glutamate neurotoxicity: mechanisms of neuroprotective treatment against oxidative stress. Ann. Neurol. *44*, 110–119.

Saxena, S., Roselli, F., Singh, K., Leptien, K., Julien, J.P., Gros-Louis, F., and Caroni, P. (2013). Neuroprotection through excitability and mTOR required in ALS motoneurons to delay disease and extend survival. Neuron *80*, 80–96.

Selvaraj, B.T., Livesey, M.R., Zhao, C., Gregory, J.M., James, O.T., Cleary, E.M., Chouhan, A.K., Gane, A.B., Perkins, E.M., Dando, O., et al. (2018). C9ORF72 repeat expansion causes vulnerability of motor neurons to Ca^{2+}-permeable AMPA receptor-mediated excitotoxicity. Nat. Commun. *9*, 347.

Sherman, S.P., and Bang, A.G. (2018). High-throughput screen for compounds that modulate neurite growth of human induced pluripotent stem cell-derived neurons. Dis. Model. Mech. *11*, dmm031906.

Shi, Y., Lin, S., Staats, K.A., Li, Y., Chang, W.H., Hung, S.T., Hendricks, E., Linares, G.R., Wang, Y., Son, E.Y., et al. (2018). Haploinsufficiency leads to neurodegeneration in C9ORF72 ALS/FTD human induced motor neurons. Nat. Med. *24*, 313–325.

Shibuya, K., Park, S.B., Geevasinga, N., Menon, P., Howells, J., Simon, N.G., Huynh, W., Noto, Y., Götz, J., Kril, J.J., et al. (2016). Motor cortical function determines prognosis in sporadic ALS. Neurology *87*, 513–520.

Šišková, Z., Justus, D., Kaneko, H., Friedrichs, D., Henneberg, N., Beutel, T., Pitsch, J., Schoch, S., Becker, A., von der Kammer, H., and Remy, S. (2014). Dendritic structural degeneration is functionally linked to cellular hyperexcitability in a mouse model of Alzheimer's disease. Neuron *84*, 1023–1033.

Stacey, P., Wassermann, A.M., Kammonen, L., Impey, E., Wilbrey, A., and Cawkill, D. (2018). Plate-Based Phenotypic Screening for Pain Using Human iPSC-Derived Sensory Neurons. SLAS Discov. *23*, 585–596.

van Zundert, B., Peuscher, M.H., Hynynen, M., Chen, A., Neve, R.L., Brown, R.H., Jr., Constantine-Paton, M., and Bellingham, M.C. (2008). Neonatal neuronal circuitry shows hyperexcitable disturbance in a mouse model of the adult-onset neurodegenerative disease amyotrophic lateral sclerosis. J. Neurosci. *28*, 10864–10874.

Vincent, F., Loria, P., Pregel, M., Stanton, R., Kitching, L., Nocka, K., Doyonnas, R., Steppan, C., Gilbert, A., Schroeter, T., and Peakman, M.C. (2015). Developing predictive assays: the phenotypic screening "rule of 3". Sci. Transl. Med. *7*, 293ps15.

Wainger, B.J., Kiskinis, E., Mellin, C., Wiskow, O., Han, S.S., Sandoe, J., Perez, N.P., Williams, L.A., Lee, S., Boulting, G., et al. (2014). Intrinsic membrane hyperexcitability of amyotrophic lateral sclerosis patient-derived motor neurons. Cell Rep. *7*, 1–11.

Wainger, B.J., Macklin, E.A., Vucic, S., McIlduff, C.E., Paganoni, S., Maragakis, N.J., Bedlack, R., Goyal, N.A., Rutkove, S.B., Lange, D.J., et al. (2021). Effect of Ezogabine on Cortical and Spinal Motor Neuron Excitability in Amyotrophic Lateral Sclerosis: A Randomized Clinical Trial. JAMA Neurol. *78*, 186–196.

Wang, D., Ji, X., Liu, J., Li, Z., and Zhang, X. (2018). Dopamine Receptor Subtypes Differentially Regulate Autophagy. Int. J. Mol. Sci. *19*, 1540.

Weiss, J.H. (2011). Ca permeable AMPA channels in diseases of the nervous system. Front. Mol. Neurosci. *4*, 42.

Weskamp, K., Tank, E.M., Miguez, R., McBride, J.P., Gómez, N.B., White, M., Lin, Z., Gonzalez, C.M., Serio, A., Sreedharan, J., and Barmada, S.J. (2020). Shortened TDP43 isoforms upregulated by neuronal hyperactivity drive TDP43 pathology in ALS. J. Clin. Invest. *130*, 1139–1155.

Yang, Y.M., Gupta, S.K., Kim, K.J., Powers, B.E., Cerqueira, A., Wainger, B.J., Ngo, H.D., Rosowski, K.A., Schein, P.A., Ackeifi, C.A., et al. (2013). A small molecule screen in stem-cell-derived motor neurons identifies a kinase inhibitor as a candidate therapeutic for ALS. Cell Stem Cell *12*, 713–726.

CellPress
OPEN ACCESS

STAR★METHODS

KEY RESOURCES TABLE

REAGENT or RESOURCE	SOURCE	IDENTIFIER
Antibodies		
Chicken anti-MAP2 antibody	Abcam	Cat# ab5392; RRID:AB_2138153
PE anti-human CD56 clone B159/NCAM antibody	BD Biosciences	Cat# 555516; RRID:AB_395906
Mouse anti-human nuclei antibody clone 235-1	Millipore	Cat# MAB1281; RRID:AB_94090
Rabbit anti-Islet 1 antibody [EP4182]	Abcam	Cat# ab109517; RRID:AB_10866454
Chicken anti-GFP antibody	Abcam	Cat# ab13970; RRID:AB_300798
PE anti-human EpCAM clone EBA-1	BD Biosciences	Cat# 347198; RRID:AB_400262
Bacterial and virus strains		
One Shot Stbl3 chemically competent *E. coli*	Thermo Fisher	Cat# C737303
3rd generation lentivirus	BCH Virus Core	N/A
Chemicals, peptides, and recombinant proteins		
CGL compound library	Pfizer	N/A
Sumanirole	Sigma	Cat# SML1087
Bromocriptine	Cayman Chemical	Cat# 22260-51-1
Y-27632	Tocris	Cat# 125450
Smoothened agonist (SAG)	Calbiochem	Cat# 364590-63-6
Smoothened agonist (SAG)	Santa Cruz	Cat# sc-202814A
Retinoic acid	Sigma	Cat# R2625
L-Asorbic acid	Sigma	Cat# A4403
Dorsomorphin	Stemgent	Code 04-0024
SB-431542	Sigma	Cat# S4317
SB-431542	Cayman Chemical	Cat# 301836-41-9
LDN193189	Sigma	Cat# SML0559
SU-5402	Cayman Chemical	Cat# 215543-92-3
DAPT	Selleck Chemical	Cat# S2215
(S)-AMPA	Tocirs	Cat# 0254
Cyclothiazide	Cayman Chemical	Cat# 2259-9 6-3
human BDNF recombinant protein	Life Tech	Cat# PHC7084
Human GDNF recombinant protein	Thermo Fisher	Cat# PHC7045
Human CNTF recombinant protein	Thermo Fisher	Cat# PHC7015
EdU	Thermo Fisher	Cat# A10044
Critical commercial assays		
CellTiterGlo	Promega	Cat# G7572
Fura-2, AM	Thermo Fisher	Cat# F1221
Experimental models: cell lines		
39b iPSC (SOD(A4V)	Eggan lab (Harvard)	N/A
39b_cor iPSC (corrected control)	Eggan lab (Harvad)	N/A
C9orf72 iPSC	Coppola lab (UCLA)	N/A
Oligonucleotides		
qPCR primers (details found in 'RT-qPCR' in method details)	IDT	N/A

(*Continued on next page*)

Continued

REAGENT or RESOURCE	SOURCE	IDENTIFIER
Recombinant DNA		
Lenti-hsyn-GCaMP6s	Engle lab (BCH)	N/A
pLKO-GFP	pLKO.1 GFP shRNA was a gift from David Sabatini (Addgene plasmid #30323; http://addgene.org/30323; RRID:Addgene_30323); Sancak et al., 2008	Cat# 30323
pLKO-human DRD2_1 (CCGGGCTGG TCTACATCAAGATCTACTCGAGTAGA TCTTGATGTAGACCAGCTTTTT)	Sigma	TRCN0000011342
pLKO-human DRD2_2 (CCGGCACCA CCTTCAACATTGAGTTCTCGAGAAC TCAATGTTGAAGGTGGTGTTTTT)	Sigma	TRCN0000011343
Software and algorithms		
Cellomics scan	Thermo Fisher	https://www.thermofisher.com/us/en/home/technical-resources/software-downloads.html#cell-imaging-hcs
Biorender	Biorender.com	https://biorender.com/
Prism	GraphPad	https://www.graphpad.com/scientific-software/prism/
Vortex	Dotmatics	https://www.dotmatics.com/products/vortex
NIS-ElementsAR	Nikon	https://www.nikon.com/products/microscope-solutions/support/download/software/imgsfw/nis-ar_v43001du164.htm

RESOURCE AVAILABILITY

Lead contact

Further information and requests for resources and reagents should be directed to and will be fulfilled by the lead contact, Clifford Woolf, clifford.woolf@childrens.harvard.edu

Materials availability

This study did not generate new unique reagents.

Data and code availability

All data are available from the lead contact upon reasonable request.

EXPERIMENTAL MODEL AND SUBJECT DETAILS

Motor neuron differentiation and maintenance

For phenotypic screen, iPSC were expanded using Essential 8^{TM}-Flex medium (Thermo Fisher), then differentiated into motor neurons using an embryonic body ("EB") based protocol as previously described (Kiskinis et al., 2014). Briefly, iPSC colonies were dissociated to single cells with accutase and plated in suspension in low-adherence flasks, at a 400,000 cells/ml density with 10 μM ROCK inhibitor (Y-27632) in Essential 8-Flex media for 24 hr. Embryoid bodies were formed and media was gradually diluted (50% on day 3 and 100% on day 4) with KOSR (DMEM/F12, 15% KOSR) between day 1 and 4 and with a neural induction medium (NIM: DMEM/F12 with L-glutamine, NEAA, Heparin (2 μg/ml), N2 supplement (GIBCO^{TM}, Thermo Fisher)) on days 5–24. Treatment with small molecules and recombinant proteins is as follows: on day 1–6, 10 μM SB431542 + 1 μM Dorsmorphin; and on day 5–24, 10 ng/ml BDNF, 0.4 μg/ml ascorbic acid, 1 μM Retinoic Acid and 1 μM Smoothened Agonist (SAG) . At day 24, EBs were dissociated to single cells with accutase, frozen and stored in liquid nitrogen until used or directed enriched through negative sorting by EpCAM antibody.

For calcium influx examination, patch clamp validation, and neuronal survival study, a modified adherent cell based protocol was used (Klim et al., 2019). Stem cells were plated in matrigel coated plates and maintained in StemFlex media (Thermo), and dissociated to single cells by accutase before differentiation. Then cells were changed to the differentiation media: DMFM12/Neurobasal 1:1, supplemented with N2, B27, Non-essential-amino-acid and glutamax. For the first 6 days of culture, the neuronal differentiation media was supplemented with SB431542 (10uM), LDN (0.1uM), retinoic acid (1uM), SAG (1uM), and switched to retinoic acid (1uM), SAG

(1uM), SU5402 (4uM), and DAPT (5uM) for the next 8 days. Then cells were dissociated by accutase, frozen and stored in liquid nitrogen until used or enriched through magnetic sorting using anti-NCAM antibody.

Motoneuron-glial cocultures

Glial cells were obtained from C57BL/6 mouse pups (age: P0-P2, box sexes) (Jackson Laboratory) and were prepared by the methods as described in previous literature (Di Giorgio et al., 2008). Briefly, postnatal cortices were dissected and trypsinized, and cells were cultured in MEMα medium (Corning, #10022-CV) supplemented with horse serum for two weeks before use. All procedures are approved by IACUC of Boston Children's Hospital. Magnetic sorted motor neurons were plated with mouse p0-2 cortical glia on PDL (100 μg/ml) and Laminin (5 μg/ml) pre-coated plates in motor neuron media (Neurobasal media) (NB, Invitrogen, Carlsbad, CA), supplemented with B27, N2 supplement, glutamax and non-essential amino acid (GIBCO™, Thermo Fisher), 10 ng/ml each of BDNF, GDNF, and CNTF, and 0.2 mg/ml ascorbic acid was replaced every 3 or 4 days.

METHOD DETAILS

Magnetic cell sorting

Frozen motor neurons were thawed and re-suspended in motor neuron (MN) media and filtered through a 70 μm filter. The cell suspension was incubated with primary PE Mouse Anti-Human EpCAM (negative selection, 1:10; BD Biosciences) or NCAM (positive selection, 1:10; BD Biosciences) in MACS buffer on ice for 15 minutes. Next, anti-PE-magnetic beads (1:10; BD Biosciences, # 557899) in MACS were added for 30 minutes at room temperature. MNs were negatively sorted to clear progenitor cells or positively sorted to retain neurons by running the total cell suspension over a MS-magnetic cell strainer column (Miltenyi Biotec).

Pfizer chemogenomic library

The Pfizer CGL3 library contains 2899 compounds (2882 of them are distinct) pre-annotated for defined targets. In order to select the most appropriate pharmacological modulator for key druggable gene families, multiple parameters of a compound are evaluated including selectivity, permeability, solubility, and cytotoxicity. CGL3 library compounds all showed potency against their primary annotated target at a concentration of less than 500 nM. Different compounds with similar targets are selected when available to increase the confidence (Jones and Bunnage, 2017). Compound's primary targets are manually annotated by Pfizer medicinal chemists based on their expert knowledge of gene families; secondary target annotations are based on the target binding activity data (IC_{50}, Ki, EC_{50}) from Pfizer internal screenings and literature data collected by CHEMBL database.

GCaMP live imaging

Magnetic sorted ALS motor neurons carrying the *SOD1(A4V)* mutation (derived from the 39b line) were plated with mouse p0-2 cortical glia 384 well Greiner Bio-one cell culture plates. Motor neurons were plated at a concentration of 7,500 cells/well and glia at a concentration of 10,000 cells/well in the presence of 10 μM ROCK inhibitor Y-27632 and 1μM EDU. Cells were maintained for 3-4 weeks to reach maximum excitability (Wainger et al., 2014).

LV-synapsin-GCaMP6 viral infections were performed in week 2 and 3 at an MOI of 5. After 3-4 weeks, synaptic blockers are added to each well at the following concentrations: Bicuculline 25μM, Strychnine 10μM, AP-5 100μM, CNQX 10μM. After 2hr chemogenomic library compounds were added at a final concentration of 3μM. DMSO was used as a negative control at 0.03%. Tetrodotoxin 5μM in 0.03% DMSO was used as a positive control. After 6hr and 24hr, the plates were recorded for 4-5hr in the Arrayscan™ XTI (Thermo Fisher) using the compartmental analysis protocol with excitation at 485 nm and emission at 521 nm, exposed for around 50 ms. Time dependent fluorescence kinetics were measured with the Arrayscan software (Thermo Scientific HCS Studio: Cellomics Scan). Objects were selected based on fluorescent intensity, shape and size, and responses were quantified for each identified object as a change in fluorescence per second. Raw fluorescent intensity (F_t) was recorded and relative intensity was calculated against the lowest fluorescent intensity during recording (F_0) for every time-point for every cell and used to calculate the difference between every subsequent time-point (second derivative: $(F_{(t+1)} - F_{(t)})/F_0$). If this difference (second derivative) was bigger than the set peak threshold (determined based on the difference between positive and negative control, usually 10%) it was counted as a peak. The number of peaks of all cells was averaged to determine the average number of peaks per well. The threshold that resulted in the highest Z-factor was set for each plate to maximize the difference between positive and negative controls.

RNA knockdown

MISSION shRNA constructs targeting human DRD2 gene were purchased from Sigma, and lentivirus was prepared and concentrated via Virus Core in Boston Children's Hospital. Virus was added into culture 1-2 weeks after plating, and the media was changed after 24h. A lentiviral construct targeting GFP gene using the same pLKO backbone was used as a control (Sancak et al., 2008).

RT-qPCR

Total RNA was extracted from cell culture using RNeasy Micro Kit (QIAGEN) and cDNA was subsequently generated using Superscript Vilo Synthesis Kit (Invitrogen) according to manufacturer's manuals. qPCR was run on Applied Biosystems 7500 machine (Life Technologies) using Fast SYBR Green Master Mix (Roche). Primers used in this study are:

GRIA1_F: acgGTTTGGGATATTCAACAGTTTGTGGTTCTC
GRIA1_R: cgtGACCTGGGAGAAATGTCACATCCTT
GRIA2_F: cgaTAAAGAGTTTTTCAGGAGAT
GRIA2_R: cgtCAGAGGGCTCCGCACTCCGCATGT
GRIA3_F: cgaCCATCAGCATAGGTGGACTTTTCAT
GRIA3_R: tcgGTTGTATAACTGCACGGCAAAGC
GRIA4_F: cgaCTAGAAAGGTTGGTTACTGGAATGATATG
GRIA4_R: cgtGCTGTGTCATTGCCAAGAGTT

Toxicity assay (CellTiterGlo)

Magnetic sorted ALS motor neurons derived from iPSC were cultured with mouse p0-2 cortical glia in 384 well plates. After 3.5 weeks, cells were treated with a concentration range of compounds in motor neuron media. After 48hr, cell survival was determined using the CellTiter-Glo 2.0 kit (Promega) kit according to manufacturer's instructions.

IC_{50} calculation

The mean and standard deviation of the HPE (100% effect) and ZPE (0% effect) were calculated for each plate. The compound data at each concentration was converted into % effect, using the ZPE and HPE controls as 0% and 100% activity, respectively. The formula used for converting each well reading into % effect is: (Well activity value – ZPE activity value) X 100/(HPE activity value-ZPE activity value). Then the % effect was plotted against log10 [compound]. An unconstrained sigmoid curve was thus fitted using a 4 parameter logistic model, and an IC_{50} was reported as the midpoint of the curve.

Multiple electrode array analysis

ALS motor neurons derived from iPSC (50,000 cells per well) were cultured with mouse p0-2 cortical glia (40,000 cells per well) in M768-KAP-96 well plates (Axion Biosystems). Using the Maestro recording system of Axion Biosystems, spontaneous motor neuron action potentials were recorded with a 200 Hz high pass and 2500 Hz low pass filter and an adaptive spike detection threshold set at 5.5 times the standard deviation for each electrode with 1 s binning. Average spike rate per electrode was determined for each well (Hz).

Enrichment analysis

Target enrichment analysis was performed by following the methodology described in Stacey et al. (2018) (Figure S3A). Briefly, for each annotated target, Fisher's exact test was performed to detect whether their ligands were significantly enriched in the IC_{50} confirmed hits from the phenotypic screen. The p value would indicate a potential association between this target and the observed phenotype. To complement the statistical hypothesis testing, Enrichment Factor was also used to indicate the effect size, by calculating the odds of hits enriched in compounds that are active against a target versus in compounds that are inactive against this target.

Immunocytochemistry

Differentiated motor neurons were cultured with glial for 4 weeks then cells were fixed, and stained by anti-human nucleus (1:1000, Millipore,), anti-MAP2 (1:4000, Abcam,), anti-GFP (1:2000, Abcam,) and anti ISL1 (1:1000, Abcam,) antibodies. Images were acquired and analyzed by the Arrayscan^{TM} XTI (Thermo Fisher) or Nikon Ti-Eclipse.

Patch clamp recording

Whole cell patch-clamp recordings were performed at room temperature in an external solution containing 145 mM NaCl, 5 mM KCl, 2 mM $CaCl_2$, 1 mM $MgCl_2$, 10 mM glucose, and 10 mM HEPES (pH 7.4). Recording electrodes (2-5 MΩ) were filled with an internal solution containing 135 mM K-Gluconate, 10 mM KCl, 1 mM $MgCl_2$, 5 mM EGTA, and 10 mM HEPES (pH 7.2). For voltage-clamp recordings, currents were elicited by 3 s polarizing steps from a holding potential of −80 mV to test potentials ranging from −80 mV to 50 mV in 10 mV increments to study the current-voltage relationship, using an Axopatch 200B amplifier (Axon Instruments). For current-clamp recordings, membrane potential was hold at −65 mV and a depolarizing current ramp (0 to 200 pA in one second) was applied to induce action potentials, or hold at around −50 mV to monitor spontaneous firing. Only neurons displaying mature morphology and big sodium currents (> 1nA) were chosen. Data were low-pass filtered at 2 kHz, digitized at 20 kHz, and analyzed using the pCLAMP 10 software suite (Molecular Devices).

Calcium response imaging

To study AMPA induced calcium response, 4-week old neurons in culture were loaded with 10 μM Fura-2-AM (Life Technologies) at 37°C for 30-45 min, washed into Standard Extracellular Solution (SES, 145 mM NaCl, 5 mM KCl, 2 mM $CaCl_2$, 1 mM $MgCl_2$, 10 mM glucose, 10 mM HEPES, pH 7.5), and imaged at room temperature. Cells were illuminated by an UV light source (Xenon lamp, 75 W, Nikon), 340 nm and 380 nm excitation alternated by a LEP MAC 5000 filter wheel (Spectra services), and fluorescence emission at 510 nm captured by Cool SNAP ES camera (Princeton Instruments, NJ, USA). Compounds were flowed directly onto neurons for 15 s

using perfusion barrel followed by SES washout (45 s), and most signals can return to the base line within 1 min. Neurons with big soma size and many neurites were selected for analysis: 340/380 ratiometric images were processed, background corrected, and analyzed with NIS-ElementsAR software (Nikon).

QUANTIFICATION AND STATISTICAL ANALYSIS

For compound confirmation on MEA, Fisher's exact test was performed for each compound to detect whether they behaved significantly different from the negative control. MEA hits were then selected based on the resulting p value (with Benjamini and Hochberg correction) ($p \leq 0.05$). Students' t test or two-way ANOVA was used for other assays, with replicates from distinct samples. Please note that statistical details are found in the figure legends.